Simultaneous optical signal to noise ratio and symbol rate estimation with blind chromatic dispersion compensation for auxiliary amplitude modulation optical signals

Junyu Wei (魏俊宇)*, Jiangyi Qin (覃江毅), Zhiping Huang (黄芝平), and Xiaojun Guo (郭晓俊)

College of Mechatronics Engineering and Automation, National University of Defense Technology, Changsha 410073, China

**Corresponding author: davidjuyun@163.com*

Received March 15, 2016; accepted July 1, 2016; posted online August 3, 2016

Based on the peak to valley ratio (PTVR) of the average magnitude difference function (AMDF), we present a novel optical signal to noise ratio (OSNR) and symbol rate (SR) estimation method for commonly used auxiliary amplitude modulations (AAMs). Moreover, it is demonstrated that the influence of chromatic dispersion (CD) on the method can be mitigated by maximizing the PTVR of the AMDF with additional tunable dispersion compensators. The results of simulations show that the OSNR estimation error can be kept within 0.8 dB in the wide OSNR range of (12, 32) dB, while the SR estimation error is below 0.079% for four widely used 10 Gsymbol/s AAM signals.

OCIS codes: 060.0060, 060.2330, 060.4510.
doi: 10.3788/COL201614.090603.

With regard to optical transport networks (OTNs) nowadays, optical signal to noise ratio (OSNR) has been popularly applied as an important index such as an assessment of the received optical signal, fault diagnosis of the fiber link, and monitoring of reconfigurable optical networks[1–4]. Therefore, OSNR estimation is an indispensable part of a fiber management system. Due to the rapid development of wideband internet services and the demand for data processing at a greater capacity, the efficient use of the optical signal spectrum and capacity is continuously being enhanced by upgrading the transport symbol rate (SR) in the OTNs. Consequently, optical hybrid modulated signals with various SRs exist in today's OTNs. Hence, the SR estimation is an urgent requirement and the first step for OTN performance monitoring[5]. In addition, OSNR and SR estimation are very useful for the realization of cognitive optical networking (CON), where the net nodes have the capability to self-detect and self-prevent errors[6].

Recently, various OSNR estimation methods have been proposed based on asynchronous delay-tap sampling (ADTS) for unnecessary clock recovery consideration and easy implementation in reality. Khan *et al.*[7,8] have demonstrated the utilization of half symbol delay-tap sampling coupled with the statistical characteristics of 38 Gbit/s return-to-zero (RZ) differential quadrature phase-shift keying (DQPSK) signals for OSNR monitoring. However, this method requires the accurate SR estimation of the received signal. In Refs. [9,10] the single channel sampling technique and variable phase difference phase portrait are used to estimate the OSNR to reduce the cost and complexity in the monitoring system. Nevertheless, the proposed method is sensitive to the distortion induced by chromatic dispersion (CD), thereby limiting its application in practice. By extracting parameters from ADTS histogram plots with 3-order polynomial fitting, Wang *et al.*[11] have proposed a method to realize the optimal OSNR monitoring of 10 Gbit/s not-return-to-zero (NRZ) on-off keying (OOK), but it is not applicable for the advanced modulation formats such as RZ-DQPSK and RZ 16-ary quadrature amplitude modulation (QAM). Similarly, several SR estimation schemes have been proposed and verified. In Ref. [12] the usage of the second autocorrelation function (ACF_2) coupled with the ADTS technique are validated for SR estimation of the simple modulation format, but for the advanced modulation format (for example, RZ-DQPSK), the ACF_2 periodicity is very sensitive to auxiliary amplitude modulation (AAM). Thus, an incorrect SR estimation result may be obtained. To solve this problem, Cui *et al.*[13] utilize the first-order autocorrelation function (ACF_1) to replace ACF_2 thanks to the stronger periodicity for those AAM signals. However, one disadvantage for these two methods is that the realization of ACF-based SR estimation requires multiple multiplications in each SR estimation process that will increase the computational time and hardware logical resources in the digital signal processor (DSP). Another drawback of the existing methods is that OSNR and SR estimation are performed according to two independent steps, which enhances the operation complexity in practice.

In this Letter, a method based on the peak to valley ratio (PTVR) of the average magnitude difference function (AMDF) is creatively proposed for simultaneous OSNR and SR estimation of multiple AAMs and data rates. Moreover, CD can be effectively compensated by maximizing the PTVR of the AMDF with a high-resolution tunable dispersion compensator (TDC). The numerical simulations are performed on VPI 9.1[14] software for

simulating a heterogeneous OTN that transmits several different widely used optical signals. To evaluate the effect of impairments on our proposed method, AMDFs are generated in the wide range of the OSNR, CD, and first-order polarization mode dispersion (PMD), respectively.

The structure of the OSNR and SR estimation system for the proposed method is shown in Fig. 1. Four different 10 Gsymbol/s AAM optical signals, including RZ-OOK, RZ-DPSK, RZ-DQPSK, and RZ-16QAM are transmitted over a single-mode fiber (SMF). The transmitted data is a pseudorandom bit sequence (PRBS) and the laser power is 1 mW. The OSNR is regulated by an erbium-doped fiber amplifier (EDFA) and a variable optical attenuator (VOA), while CD and differential group delay (DGD) are changed by a CD and first-order PMD emulator. The angle between the principal states of polarization (PSP) of the PMD emulator and the different modulation optical signal's state of polarization (SOP) is 45°. Then the optical signal is split at a fixed power by an optical coupler and filtered by an optical bandpass filter (OBPF) to get the demand channel signal. Afterward, the filtered optical signal is directly detected by a positive intrinsic-negative (PIN) diode to get the received electrical signal. The bandwidths of the OBPF, PIN detector, and analog-to-digital convertor (ADC) are 0.8 nm, 50 GHz, and 30 GHz, respectively.

The received electrical signal is sampled asynchronously at the sampling frequency $f_s = 500$ MHz, which is much slower than the bit rates of all four AAM signals. A total of $N = 4096$ sampled data pairs, including $X_1 = X(t_i)$ and $X_2 = X(t_i + \Delta\tau)$, are obtained for each delay, while the delay-tap time $\Delta\tau$ is changed from 0 to 350 ps. A large fixed delay of 24.5 ns is introduced to offset X_1 and X_2 so that the AMDF waveform is clearer and less sensitive to transmission impairments. Essentially, X_1 and X_2 have the same AAH distribution because X_1 and X_2 are sampled from the same signal waveform. Hence, AMDF can be defined as

$$\mathrm{AMDF}(\Delta\tau) = \frac{1}{N}\sum_{1}^{N}\left|\frac{X_1 - X_2}{\sigma}\right|, \tag{1}$$

where σ is the standard deviation of $X_{1,2}$. In view of the amplitude periodic characteristics of AAM signals, the minimum value (the valley point in the AMDF waveform) can be obtained when the delay-tap time equals the symbol period. Additionally, the AMDF is generated from the sum of the absolute differential value of the asynchronous sampling of data pairs. Compared to the SR estimation based on ACFs[12,13], AMDF-based estimation can effectively save the logical resources and computational time due to the fact that it utilizes subtraction rather than multiplication.

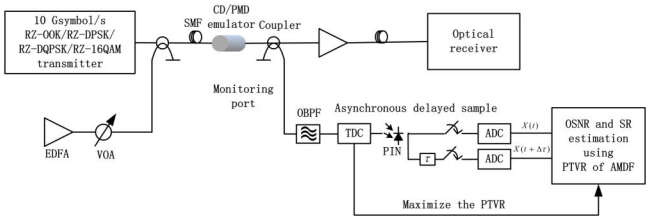

Fig. 1. System structure for OSNR and SR estimation using the PTVR of the AMDF.

Figure 2 shows AMDF raw data and 8-order Fourier series fitting curves under different OSNRs for four commonly used 10 Gsymbol/s AAMs. Whatever the AMDFs are under different OSNR levels, it can be found that the AMDFs show explicit periodicity equal to the symbol duration period of 100 ps. In Fig. 2, as variations of the AMDF waveform tend to be smooth and steady after the first valley, the second valley and the third peak points of the AMDF waveform are selected to determine the PTVR, which is derived from

$$\begin{aligned}\mathrm{PTVR} &= \left|\frac{\mathrm{AMD}F_{\max}}{\mathrm{AMD}F_{\min}}\right| = \left|\frac{\mathrm{AMDF}\left(\frac{T_{\mathrm{symbol}}}{2}\times I\right)}{\mathrm{AMDF}(T_{\mathrm{symbol}}\times I)}\right| \\ &= \left|\frac{\frac{1}{N}\sum_1^N\left|\frac{X_1-X_2}{\sigma}\right|_{\frac{T_{\mathrm{symbol}}}{2}}}{\frac{1}{N}\sum_1^N\left|\frac{X_1-X_2}{\sigma}\right|_{T_{\mathrm{symbol}}}}\right| = \left|\frac{E[|X_1-X_2|]_{\frac{T_{\mathrm{symbol}}}{2}}}{E[|X_1-X_2|]_{T_{\mathrm{symbol}}}}\right|,\end{aligned} \tag{2}$$

where T_{symbol} is the symbol period and $I \in \{1, 2, 3\ldots\}$ is a positive integer. Hence, the PTVR of the AMDF can be considered as a statistical feature of the received signal amplitude waveform in the time domain. According to Fig. 3, the PTVRs appear larger when the OSNR = 24 dB than when the OSNR = 16 dB for all four modulation formats. Because the higher OSNR means a better received signal waveform, the difference between the delayed sampling pairs $X_1 = X(t_i)$ and $X_2 = X(t_i + \Delta\tau)$ in a symbol period or two adjacent symbols is distinctive.

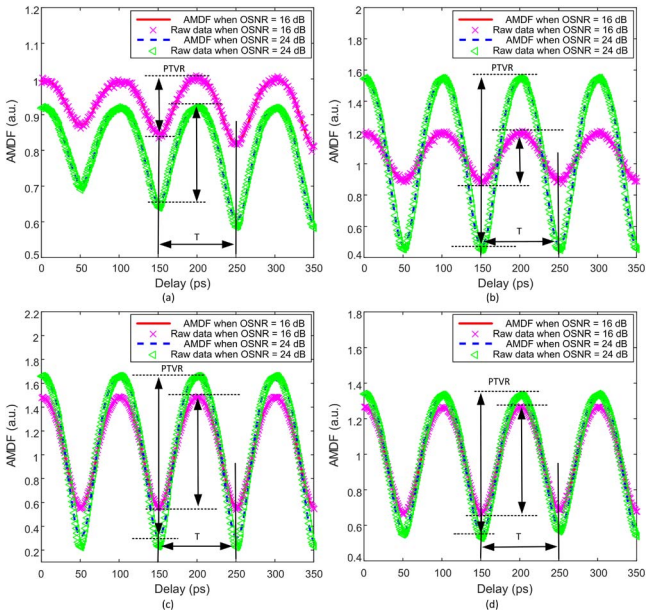

Fig. 2. Raw data and 8-order Fourier fitting plot of the AMDF for 10 Gsymbol/s (a) RZ-OOK, (b) RZ-DPSK, (c) RZ-DQPSK, and (d) RZ-16QAM.

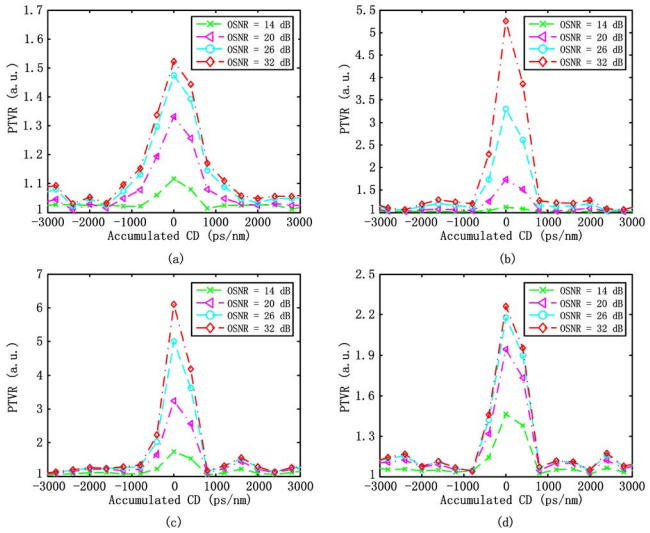

Fig. 3. PTVR versus accumulated CD for 10 Gsymbol/s (a) RZ-OOK, (b) RZ-DPSK, (c) RZ-DQPSK, and (d) RZ-16QAM.

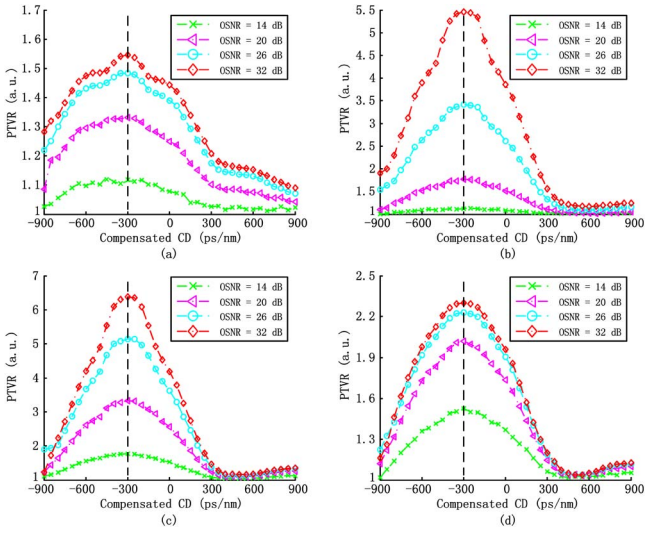

Fig. 4. Variations of the PTVR versus compensated CD when the actual CD = 300 ps/nm for 10 Gsymbol/s (a) RZ-OOK, (b) RZ-DPSK, (c) RZ-DQPSK, and (d) RZ-16QAM.

For long-haul OTN, it is indisputable that the performance of OSNR and SR estimation will degrade as a result of a large residual CD[15]. Thus, it is an urgent requirement of accurate CD compensation to ensure the reliability of the proposed method. The variations of the PTVR versus accumulated CD are plotted in Fig. 3. We can find that the PTVR decreases along with CD accumulation in the positive and negative two directions and finally saturates. Most importantly, different OSNRs only affect the peak amplitude of the PTVR but not the peak position, which always appears near CD = 0 ps/nm. Hence, it is expected that a large residual CD can be compensated by maximizing the PTVR with a high-resolution TDC module. Additionally, it is noted that the PTVR curves become flat when the OSNR is very low (e.g., RZ-DPSK) because the ASE noise is the main effect on the received signal instead of the accumulated CD.

The setup is similar to that shown in Fig. 1. The TDC module with a tuning resolution of 10 ps/nm is utilized to implement the dynamic CD compensation by maximizing the PTVR. Before the OSNR estimation, the TDC is tuned in the range from −900 to 900 ps/nm in steps of 50 ps/nm. In each OSNR estimation a total of 51609600 asynchronous sampling pairs are utilized to calculate the PTVRs corresponding to different compensated CDs. Finally, 36 PTVRs are compared and the maximum PTVR is selected for OSNR monitoring. Figure 4 shows the variations of the PTVR versus the compensated CD, when the actual CD is 300 ps/nm. From the figure it is clear that the peak position of the PTVR moves to the nearby compensation value of −300 ps/nm, but the amplitude peak of PTVR is only relative to the OSNR.

Considering the ASE noise for a low OSNR and the receiver thermal and shot noise for a high OSNR, OSNR is changed from 12 to 32 dB in steps of 1 dB. Numerical simulations are performed on the system using the procedure described in Fig. 1. Consequently, Fig. 5 shows the PTVR versus the OSNR for four different modulated signals. According to Fig. 5 there are two noteworthy points. First, we observe that the raw PTVR data of four modulation formats quasi-linearly rise along with the increase of the OSNR over most of the monitoring range, thereby availing good sensitivity over the wide monitoring range. Second, with the increase of the actual OSNR, the measured PTVR increases continuously without saturation even when the OSNR is larger than 32 dB in RZ-DPSK and RZ-DQPSK. Moreover, the dynamic range of the PTVR in these two modulation schemes is much higher than those in RZ-OOK and RZ-16QAM. To evaluate the error between the estimated values and

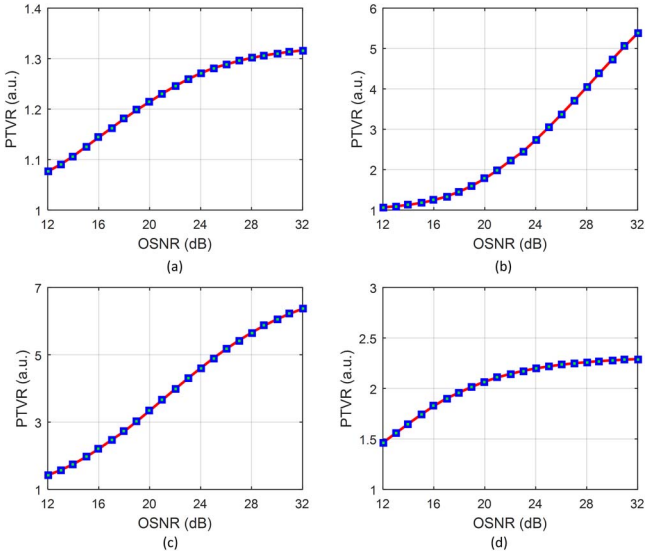

Fig. 5. PTVR raw data versus the OSNR for 10 Gsymbol/s (a) RZ-OOK, (b) RZ-DPSK, (c) RZ-DQPSK, and (d) RZ-16QAM.

the actual OSNRs, we adopt the 5-order polynomial fitting to convert the PTVR ranges among (12–32) based on the root mean squared error (RMSE) and adjust R-square (Adj. R-Square) algorithms (Table 1)[9,11]. Consequently, the following estimated OSNR mathematical expression can be given:

$$\mathrm{OSNR}_{\mathrm{est}} = p5 \times \mathrm{PTVR}^5 + \cdots + p1 \times \mathrm{PTVR} + p0. \quad (3)$$

In addition, the OSNR estimation error induced by 5-order polynomial incomplete fitting and imperfect compensation of TDC is investigated, which is considered as self-error for our proposed estimation system. The coefficients of polynomial fitting are computed based on the PTVRs when CD = 0 ps/nm as standard equations. In the different OSNR estimation cases, the CD value randomly selects in the compensation step range −50 to +50 ps/nm, and each $F_{\mathrm{OSNR\_est}}$ for every different OSNR is the average value of 50 times.

As shown in Fig. 6(a), $F_{\mathrm{OSNR\_est}}$ after blind residual dispersion compensation is plotted as a function of the actual OSNR and it can be regarded as the corresponding estimated OSNR. Figure 6(b) displays the estimation error versus the actual OSNR. It is evident that the estimation error keeps within 0.8 dB among the actual OSNR range from 12 to 32 dB for four modulations. It can be predicted that the estimation performance can be improved by increasing the number of fitting samples and using a smaller step of CD compensation in TDC, but the complexity and computation time are equivalent to enhance as well.

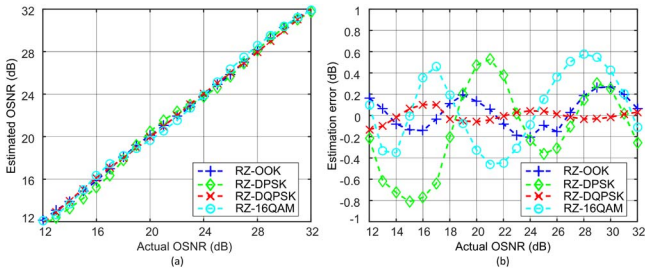

Fig. 6. (a) $F_{\mathrm{OSNR\_est}}$ versus actual OSNR; (b) the OSNR estimation error versus actual OSNR.

Table 2 summarizes the maximal errors of AMDF-based SR estimation in the OSNR range of (12, 32) dB. Compared the estimation errors corresponding to respective 10 Gsymbol/s AAM optical signals, it can be found that incorrect estimation results dramatically decline after blind CD compensation. For all four different AAMs, the overall error is below 1.75% without blind CD compensation, while 0.079% of the total error is achieved with blind CD compensation. Thus, we can believe that the blind CD compensation with TDC is profitable and reasonable for the improvement of our proposed SR estimation.

To analyze the resilience of our proposed method against first-order PMD distortion (caused by the increase of large accumulated CD), numerical simulations are operated on the optical transmission system as shown in Fig. 1. The reference OSNRs are 14, 20, 26, and 32 dB from low to high. PMD is changed in the range from 1 to 10 ps (in steps of 1 ps). Figure 7 shows the OSNR absolute estimation errors versus the variations of PMD for four different modulation formats. In Fig. 7(a), the estimation error is greater than 1 dB for the OSNR = 14 dB when PMD exceeds 4.5 ps, owing to too small of a PTVR induced by the increase of the PMD. However, the estimation error can keep as low as 0.5 dB for the better OSNRs while the PMD is as large as 10 ps. For RZ-DPSK and RZ-DQPSK in Figs. 7(b) and 7(c), respectively, the absolute estimation error fluctuates below 0.14 dB in the PMD test range as a result of the proposed method self-error. With regard to RZ-16QAM in Fig. 7(d), we note that the estimation error is less than 1 dB in the PMD scope for OSNR > 20 dB. Apart from the self-error factor, the estimation error increases because a large PMD induced the untimely saturation of a 5-order polynomial fitting. On the other side, a multilevel amplitude modulation narrows the difference between the two ADTS points in one symbol or two adjacent symbols, thus the variations of PTVR become much more sensitive to the increase of the PMD than other modulation formats.

Figure 8 shows the SR estimation error versus variations of the PMD for four different AAMs. Two points are noteworthy. First, the estimation errors corresponding to respective AAMs increase along with the PMD accumulation, especially when the OSNRs are low. Second, when

Table 1. Coefficients of 5-order Polynomial Fitting Calculated for OSNR Monitoring with Different Modulation Formats[a]

	The coefficients of 5-order polynomial fitting by RMSE and Adj. R-Square algorithms					
Modulation formats	$p5$	$p4$	$p3$	$p2$	$p1$	$p0$
RZ	1.646×10^5	-9.641×10^5	2.257×10^6	-2.639×10^6	1.542×10^6	-3.6×10^5
RZ-DPSK	0.1051	−1.998	14.64	−51.58	90.28	−41.2
RZ-DQPSK	0.02304	−0.4546	3.585	−14.05	30.44	−11.6
RZ-16QAM	3.587×10^2	-3.116×10^3	1.075×10^4	-1.842×10^4	1.566×10^4	-5.28×10^3

[a]It can be found that different modulation formats have different OSNR threshold values.

Table 2. SR Estimation Errors for 10 Gsymbol/s Different AAMs Using AMDF

Modulation formats	SR Estimation Error (%)	
	SR Rstimation Without Blind CD Compensation	SR Estimation With Blind CD Compensation
RZ-OOK	<1.5	<0.08
RZ-DPSK	<1.5	<0.082
RZ-DQPSK	<2	<0.083
RZ-16QAM	<2	<0.071

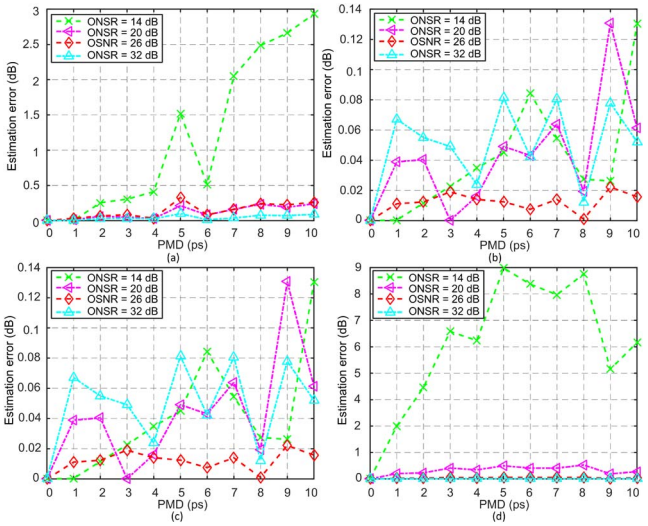

Fig. 7. OSNR absolute estimation error versus PMD for 10 Gsymbol/s (a) RZ-OOK, (b) RZ-DPSK, (c) RZ-DQPSK, and (d) RZ-16QAM.

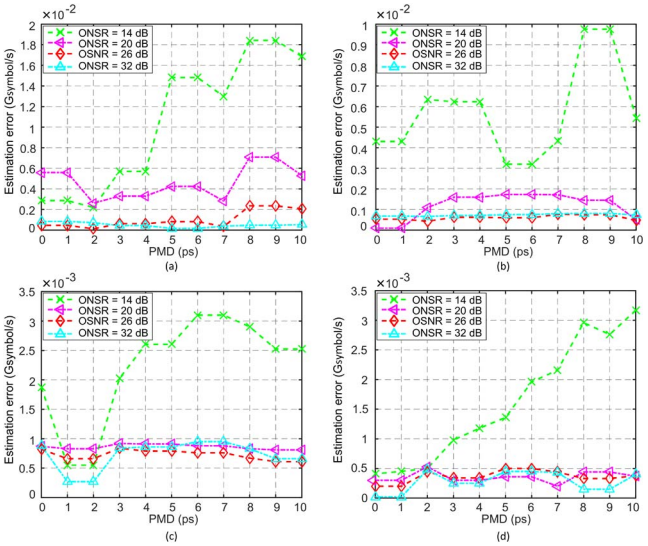

Fig. 8. SR estimation error versus the PMD for 10 Gsymbol/s (a) RZ-OOK, (b) RZ-DPSK, (C) RZ-DQPSK, and (d) RZ-16QAM.

the OSNR > 20 dB, the maximum estimation error among the four typical AAMs can keep within 0.008 Gsymbol/s while the PMD value is as large as 10 ps. As a 10 ps PMD is tantamount to tens of thousands of kilometers of fiber transmission distance with typical PMD coefficients of 0.1 $\mathrm{ps}/\sqrt{\mathrm{km}}$, the estimation errors of the proposed OSNR monitoring method still are at acceptable levels for the long or ultra-long fiber communication, in reality.

In this Letter, a competitive method using the PTVR of the AMDF is proposed for simultaneous OSNR and SR estimation with blind CD compensation of four widely used AAM optical signals. Moreover, this method is robust to PMD impairment. Furthermore, the overall OSNR and SR estimation errors of this method can be kept smaller than 0.8 dB and 0.079%, respectively, with an expanded large CD tolerance in the wide OSNR monitoring range for 10 Gsymbol/s AAM signals. Thanks to its excellent performance, this method can be utilized in the optical receivers based on the DSP as well as the intermediate transmission node of the ultra-long cognitive optical communication for the next generation optical network.

This work was supported by the National Natural Science Foundation of China (NSFC) under Grant No. 61374008.

References

1. Z. Dong, Q. Sui, A. P. T. Lau, K. Zhong, Z. L. L. Li, and C. Lu, in *Proceedings of the Optical Fiber Communication Conference* (2015).
2. W. Peng, L. Xi, X. Weng, X. Zhang, D. Zhao, and X. Zhang, Chin. Opt. Lett. **11**, 080604 (2013).
3. S. D. Dods, T. B. Anderson, K. Clarke, M. Bakaul, and A. Kowalczyk, in *Proceedings of the Optical Fiber Communication Conference* (2007).
4. Z. Q. Pan, C. Y. Yu, and E. A. Willner, Opt. Fiber Technol. **16**, 20 (2010).
5. Z. Yan, Y. Liu, and X. Chen, Chin. Opt. Lett. **12**, 100605 (2014).
6. W. Wei, C. G. Wang, and J. J. Yu, IEEE Commun. Mag. **50**, 106 (2012).
7. F. N. Khan, A. P. T. Lau, Z. Li, C. Lu, and P. K. A. Wai, IEEE Photonics. Technol. Lett. **22**, 823 (2010).
8. F. N. Khan, A. P. Tao, L. C. Lu, and P. K. A. Wai, in *Proceedings of the National Fiber Optic Engineers Conference* (2010).
9. Y. Yu, B. Zhang, and C. Yu, Opt. Express **22**, 6874 (2014).
10. Y. Yu and C. Yu, Opt. Express **23**, 11284 (2015).
11. X. Wang, X. M. Ge, Z. Ding, and Y. Xu, Opt. Commun. **341**, 237 (2015).
12. Y. Zhou, T. B. Anderson, K. Clarke, A. Nirmalathas, and K. L. Lee, IEEE Photonics. Technol. Lett. **21**, 893 (2009).
13. S. Cui, S. Jin, W. Xia, C. Ke, and D. Liu, Opt. Commun. **354**, 218 (2015).
14. VPIsystems, "VPItransmissionMaker," retrieved www.VPIphotonics.com (2013).
15. D. Xie, J. He, L. Chen, J. Tang, and M. Chen, Chin. Opt. Lett. **12**, 040604 (2014).